

Diffusion on Demand to Control Precipitation Aging: Application to Al-Mg-Si Alloys

S. Pogatscher,^{1,2,*} H. Antrekowitsch,² M. Werinos,² F. Moszner,¹ S. S. A. Gerstl,³ M. F. Francis,⁴ W. A. Curtin,⁴
J. F. Löffler,¹ and P. J. Uggowitzer¹

¹Laboratory of Metal Physics and Technology, Department of Materials, ETH Zurich, 8093 Zurich, Switzerland

²Institute of Nonferrous Metallurgy, Montanuniversitaet Leoben, 8700 Leoben, Austria

³Scientific Center for Optical and Electron Microscopy ScopeM, ETH Zurich, 8093 Zurich, Switzerland

⁴Institute of Mechanical Engineering, EPFL, 1015 Lausanne, Switzerland

(Received 18 November 2013; published 6 June 2014)

We demonstrate experimentally that a part-per-million addition of Sn solutes in Al-Mg-Si alloys can inhibit natural aging and enhance artificial aging. The mechanism controlling the aging is argued to be vacancy diffusion, with solutes trapping vacancies at low temperature and releasing them at elevated temperature, which is supported by a thermodynamic model and first-principles computations of Sn-vacancy binding. This “diffusion on demand” solves the long-standing problem of detrimental natural aging in Al-Mg-Si alloys, which is of great scientific and industrial importance. Moreover, the mechanism of controlled buffering and release of excess vacancies is generally applicable to modulate diffusion in other metallic systems.

DOI: 10.1103/PhysRevLett.112.225701

PACS numbers: 64.70.kd, 61.72.jd, 66.30.Lw, 81.40.Cd

Al-Mg-Si alloys are the most widely used age-hardenable aluminium alloys, with industrial applications in lightweight construction, automotive, aircraft, and architecture [1]. The preferential heat treatment for hardening is artificial aging via baking at ~ 430 – 460 K after quenching from ~ 800 K. However, detrimental natural aging appears within minutes of room temperature (RT) storage after quenching [2,3], making it unavoidable since there are logistical, technological, and physical time constraints in commercial production. The effect retards artificial aging kinetics by an order of magnitude and reduces the achievable strength. Consequently, the material properties, scope of applications, and energy efficiency in the production of Al-Mg-Si alloys are impaired.

Discovered 75 years ago [4], just one year after the origin of age hardening was explained [5,6], many researchers have addressed this problem since [3,7–12]. Nevertheless, the mechanisms of natural aging in Al-Mg-Si alloys and their competition with artificial aging processes remain unsolved. Excess vacancies formed upon quenching are essential for fast artificial aging [10,12] by governing the precipitation of the hardening phase β'' [13]. However, such vacancies also allow sufficient diffusion at low temperatures to cause natural aging. Thus, eliminating the negative effect of natural aging is achievable in principle by preventing excess vacancy-mediated diffusion at RT and facilitating such diffusion during elevated temperature artificial aging. Here, we demonstrate that such a diffusion on demand concept can be executed by adding trace amounts of solutes with sufficient solubility in the aluminum matrix and optimal binding energy to vacancies.

A strong binding of vacancies to solutes [14] has previously been used to explain sluggish natural aging

kinetics reported for Al-Cu alloys with additions of Sn [15]. But natural aging in Al-Cu is not deleterious and, more importantly, there has thus been no consideration of vacancy release during artificial aging—the key feature for solving the negative effect of natural aging in Al-Mg-Si alloys. For Al alloys containing Mg, it was also believed that the Sn solubility is insufficient for trapping vacancies, because of Mg_2Sn phase formation [16]. However, we are able to dissolve ~ 100 at.ppm (atomic parts per million) of Sn in the well-known Al-Mg-Si alloy AA6061 [17] at a solution treatment temperature of 843 K (see the Supplemental Material [18]). Thus, as described below, control of diffusion by the buffering and releasing of vacancies during natural and artificial aging, respectively, is realizable for Al-Mg-Si alloys and solves the 75-year-old problem of natural aging in these alloys [4] with great economic consequences for their application as lightweight alloys.

Alloys were prepared by melting an industrial AA6061 alloy (Mg 0.90, Si 0.59, Cu 0.09, Fe 0.28, Cr 0.07, Mn 0.05, Zn 0.02, and Ti 0.05, all in at.%) and adding pure Sn (99.9 at.%). Argon gas purging was applied to reduce the hydrogen content before the alloys were cast to slabs ($150 \times 90 \times 35$ mm³). To check the chemical composition, optical emission spectrometry (SPECTROMAXx from SPECTRO) was applied during the alloying procedure and to the final plates using an appropriate calibration sample as standard. After cutting and homogenization (43.2×10^3 s at 773 K and 43.2×10^3 s at 843 K), hot rolling (823 K) from 20 to 4.2 mm thickness was conducted. Solution heat treatment was performed at 843 K for 1.2×10^3 s. Subsequent quenching was carried out in water at RT, and for natural aging the samples were kept in a peltier-cooled incubator at RT. Artificial aging was carried

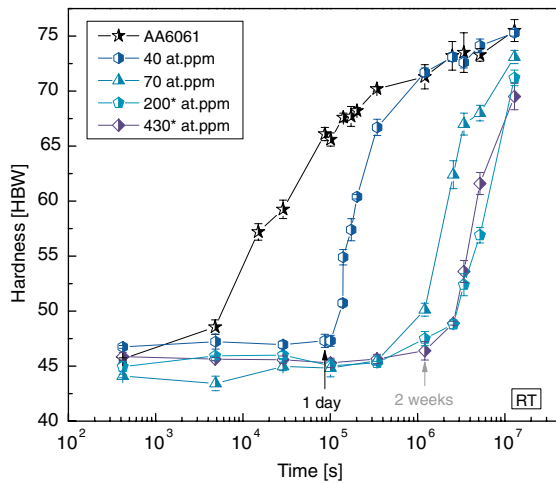


FIG. 1 (color online). Evolution of hardness during RT storage after quenching for the Al-Mg-Si alloy AA6061 with and without Sn addition. The increase in hardness is retarded with increasing the amount of Sn added. Sn additions above the solubility limit (~ 100 at.ppm) are marked with an asterisk.

out in an oil bath at 443 K. Brinell hardness measurements (HBW 2.5/62.5/15) were performed on polished samples ($17 \times 10 \times 3.4$ mm³) using an EMCO-Test M4 unit. Needle-shaped specimens for atom probe tomography [19,20] (APT) were prepared via a standard two-step electropolishing method [21]. APT was performed on a LEAPTM 4000 X HR atom probe at a specimen temperature of 23.7 K with a pulse fraction of 20%, a pulse rate of 200 kHz, and a detection rate of 1% under ultrahigh vacuum ($< 10^{-10}$ mbar). The software package IVAS 3.6.4TM from Cameca was used for the reconstruction procedure and analysis. For the calculations the Perdew-Wang-91 generalized gradient density functional theory (DFT) as implemented in VASP was used [22]. A Monkhorst-Pack k -mesh equivalent to $9 \times 9 \times 9$ in the fcc-Al cell was used with a kinetic energy cutoff of 250 eV [23]. Energy barriers were calculated using the nudged elastic band method [24]. Calculations were performed in $4 \times 4 \times 4$ cubic unit cells at fixed volume, and energy contributions due to any induced pressures were verified to be negligible. Relaxation calculations were converged to 10^{-4} eV and nudged elastic band to 0.1 eV/Å.

Figure 1 shows the effect of Sn on the evolution of hardness during RT storage after quenching from 843 K. Sn additions delay the observed hardening by orders of magnitude, from the time scale of 1 h up to several weeks, depending on the Sn content. For attempted Sn additions above the solubility limit (~ 100 at.ppm, also indicated by Sn additions marked with an asterisk) the retardation of hardening saturates, consistent with the solubility limit for Sn in the alloy at 843 K.

Since natural aging in Al-Mg-Si alloys during RT storage has been explained by the clustering of Mg and Si [11], we attribute the retardation of hardening to the

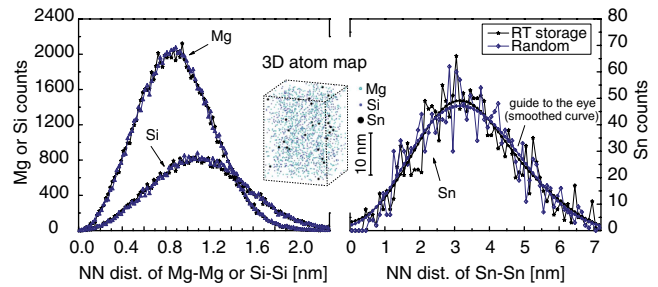


FIG. 2 (color online). Analysis of solute clustering during RT storage. Results are obtained by APT for Sn addition of 200* at.ppm and 2 weeks of RT storage after quenching. A 3D atom map of Mg, Si, and Sn (magnified) is shown. No solute clusters are recognizable by eye. (For better visibility the reader is referred to the video included in the Supplemental Material [18].) An analysis of NN distances of Mg, Si, and Sn revealed no significant difference between the measured and a calculated randomized distribution of these elements.

impeding of such cluster formation. Figure 2 shows a three-dimensional (3D) map of the positions of Mg, Si, and Sn atoms in the alloy with an addition of 200* at.ppm Sn after 2 weeks of RT storage measured by APT (see [18] for APT reconstruction details). A nearest-neighbor (NN) distribution analysis [25] shows no statistically significant difference between the measured distribution and a calculated random distribution of the solute elements. This indicates that no clusters of Mg and Si exist within the detection limit of a few atoms, which agrees well with the hardness data in

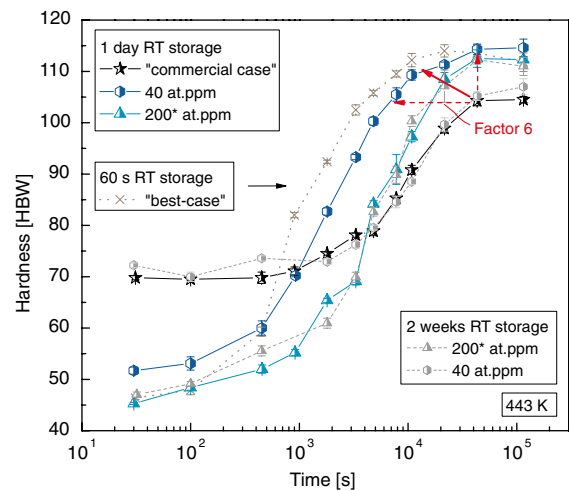


FIG. 3 (color online). Evolution of hardness during artificial aging at 443 K with and without Sn addition for various periods of RT storage. Data generated from laboratory scaled samples without Sn addition and RT storage < 60 s are shown as a “best-case” reference, where the maximum kinetics and hardening potential is achieved. This best-case scenario cannot be realized in a commercial process, where the material undergoes a significantly longer RT storage (see the commercial case in the figure; a similar curve is obtained for RT storages of 2 weeks). The negative effect of RT storage can be eliminated by minute additions of Sn, which enhance kinetics and hardness (red arrows).

Fig. 1. In addition, although data are noisy due to the very low Sn concentration, there is no hint of Sn clustering.

Figure 3 shows the evolution of the hardness in AA6061 during artificial aging at the standard temperature of 443 K after both 1 day and 2 weeks of RT storage, with and without Sn addition. Also shown are data generated from laboratory samples without Sn addition and with RT storage shorter than 60 s; even though not commercially feasible, this would be the “best-case” reference of maximum kinetics and hardening potential that can be achieved due to the absence of natural aging. The results in Fig. 3 show that Sn not only retards hardening during RT storage over orders of magnitude (Fig. 1), but it then also accelerates the kinetics during artificial aging, relative to the Sn-free “commercial case,” as shown exemplarily for AA6061 stored at RT. In fact, the hardening kinetics can even approach that of the best-case reference AA6061. The effectiveness of Sn can be controlled by the amount added and the period of RT storage. Lower Sn additions (~ 40 at.ppm) delay natural aging for a period sufficient to overcome most logistical, technological, and physical constraints in the production of semifinished Al-Mg-Si products (1 day; see Fig. 1) but then allow for artificial aging that approaches the best case and is 6 times faster than the current commercial case. Higher Sn additions at the ~ 100 at.ppm solubility limit prevent natural aging at RT even for much longer times, (e.g., 2 weeks; see Fig. 1) and still accelerate artificial aging, but somewhat less pronounced. However, at all these Sn additions, a 10% higher hardness relative to the commercial case of AA6061 is ultimately achieved.

It has been proposed that Sn could form small precipitates that act as heterogeneous nucleation sites for

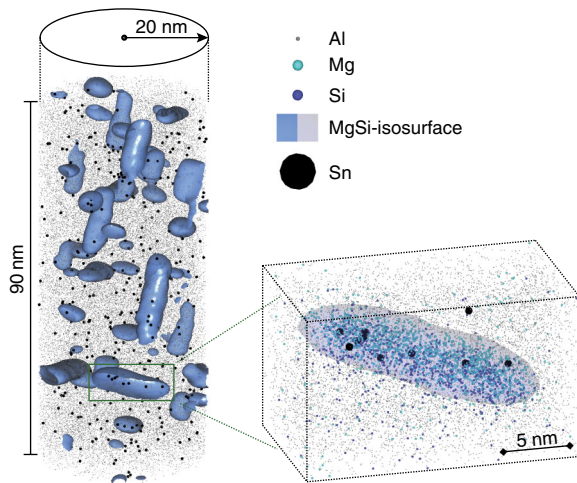


FIG. 4 (color online). Artificially aged microstructure. Data obtained by APT for Sn addition of 200* at.ppm and artificial aging of 12 h at 443 K after 2 weeks of RT storage. A 3D map of Al and Sn atoms is shown. MgSi precipitates are indicated by semitransparent isoconcentration surfaces of Mg and Si (4 at.%). Sn is found within the matrix and the MgSi precipitates and forms no individual precipitates (see magnified inset).

precipitation [26]. However, APT results for AA6061 with Sn addition of 200* at.ppm and artificial aging at 443 K after 2 weeks of RT storage reveal no small Sn precipitates (Fig. 4). Sn does appear in the MgSi precipitates, which indicates a finite solubility of Sn in the precipitates, possibly due to its tendency to bind with Mg [16]. This also suggests that Sn can diffuse during artificial aging.

Empirically, the results in Figs. 1–4 are consistent with the mechanistic concept proposed in the introduction: solutes S trap vacancies V at low temperatures and thus prevent natural aging, but release the vacancies at elevated aging temperatures, thereby allowing the desired aging processes to occur without the detrimental influence of processes that would normally happen during RT storage. This mechanistic concept is supported by thermodynamic and kinetic models using first-principles calculations of Sn-vacancy binding and vacancy migration around Sn solutes. The general thermodynamic model considers a low concentration c_S of solutes dissolved in the metal lattice, with binding energies ΔE_{SV}^i (positive values indicating binding) for various possible vacancy-solute binding complexes. Considering the solutes at fixed position in the metal lattice, we compute the concentrations c_V of untrapped vacancies and the concentrations c_{SV}^i of the vacancy-solute complexes at the effective quench temperature T_Q , where annihilation of vacancies essentially ceases [27]. As the temperature of the alloy is quenched below T_Q , further vacancy annihilation is not possible but re-partitioning of the vacancies among the untrapped and trapped solute-vacancy complexes is allowed because such trapping requires very limited vacancy transport. Any vacancy-mediated diffusional processes at temperature T are then controlled by the residual untrapped vacancy concentration $c_V(T)$, and so vacancy-mediated diffusion is retarded by a factor $R = c_V(T_Q)/c_V(T)$.

The thermodynamic model uses simple solution theory, which includes only the entropy due to mixing, and assumes low concentrations $c_V, c_S \ll 1$. Rather than present the detailed model (see the Supplemental Material [18] for a full presentation), we show here a simplified model that is numerically accurate for Sn. The simplified model assumes that one S can bind only one V at a time with a binding energy ΔE_{SV} , at one of the 12 NN sites of the S atom in the fcc lattice, and that the total quenched vacancy concentration is much smaller than the solute concentration, $c_V^{\text{tot}}(T_Q) \ll c_S$. At any temperature $T < T_Q$, the total concentration of V in the material is fixed at $c_V^{\text{tot}}(T_Q)$, i.e., $c_V^{\text{tot}}(T_Q) = c_V(T) + 12c_S c_{SV}(T)$. Furthermore, the ratio of the trapped and untrapped V concentrations is governed by the Boltzmann factor, $c_{SV}(T)/c_V(T) = e^{\Delta E_{SV}/kT}$, where k is Boltzmann's constant. Combining the above two equations yields

$$R = \frac{c_V(T_Q)}{c_V(T)} = \frac{1 + 12c_S(e^{\Delta E_{SV}/kT})}{1 + 12c_S(e^{\Delta E_{SV}/kT_Q})}. \quad (1)$$

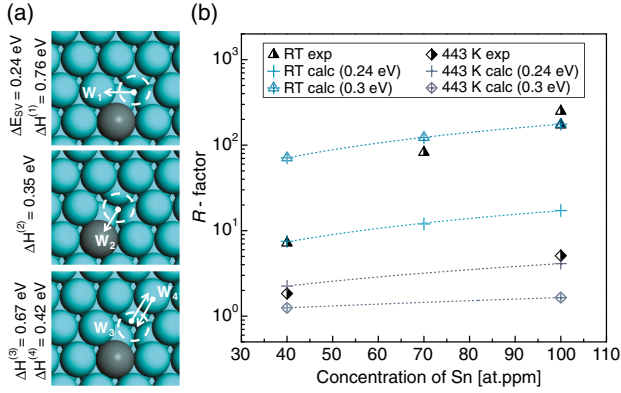


FIG. 5 (color online). (a) DFT results for the Sn-V configuration. The binding energy and the migration barriers relevant to assess Sn diffusion within the context of the five-frequency model are shown. (b) Comparison of the rate reduction R factor calculated from Eq. (2) using two different values for ΔE_{SV} (as calculated, and as to fit experiments) and experimental R values deduced from Figs. 1 and 3, for Sn at concentrations of 40, 70, and/or 100 at.ppm at RT and artificial aging temperature. The model captures the major trends shown experimentally: R is significant at RT and at the Sn solubility limit, but is fairly small at the artificial aging temperature.

This ratio is unity in the limits of zero V - S binding, $T = T_Q$, or $c_S = 0$, as necessary physically.

For Sn in Al, we have computed the binding energies ΔE_{S-V}^i using quantum DFT for an S - V pair, an S - V - V triplet where the vacancies are NN of each other, and of various V - S - V triplets where the vacancies are not NN. The value of ΔE_{SV} shown in Fig. 5(a) agrees well with previous DFT calculations [14,28]. For Sn, the calculated binding energies indicate that the V - S - V complexes are negligible but the S - V - V complexes are not (see [18] for the values). Nonetheless, a full analysis shows that the net effect of the S - V - V complexes on trapping and on R is small, and that the second term in the denominator of Eq. (1) is negligible for all reasonable quenching temperatures ($600 \text{ K} < T_Q < 800 \text{ K}$). Thus, over a range of temperatures, and for sufficient Sn concentrations, the retardation factor is approximately

$$R = 1 + 12c_S(e^{\Delta E_{SV}/kT}), \quad (2)$$

which is conveniently independent of the effective quenching temperature and the quenched vacancy concentration $c_V^{\text{tot}}(T_Q)$.

Figure 5(b) shows the approximate factor R computed using Eq. (2) for Sn at concentrations of 40, 70, and/or 100 at.ppm at both RT and 443 K (artificial aging), using the V -Sn binding energy determined by DFT. R is significant at RT and at the Sn solubility limit, but is fairly small at the artificial aging temperature. Thus, trapping of V by Sn suppresses RT aging processes significantly but has a much smaller effect on artificial aging. Figure 5(b) also

shows the R value from experiments, computed as the ratio of the times required to achieve 50% of the hardening with and without Sn, respectively. Such an experimental R value assumes that all aging processes are kinetically limited by vacancy-mediated diffusion, which is the mechanism proposed here. Quantitatively, the R values obtained using the DFT-computed V -Sn binding energy are somewhat smaller than measured. Better quantitative agreement can be obtained using a larger V -Sn binding energy, as shown in Fig. 5(b) for $\Delta E_{SV} = 0.3 \text{ eV}$ which is within the range of experimentally derived values [29]. While the differences between the computed and deduced binding energies remain to be resolved, the model nonetheless captures the major trends shown experimentally.

The above model is applicable if the V - S complex cannot diffuse rapidly. For the Sn- V pair we have computed, using DFT and the nudged elastic band method [24], all of the migration barriers relevant for assessing Sn diffusion within the context of the five-frequency model [30], as shown in Fig. 5(a). Application of the five-frequency model to Sn, neglecting differences in the vibrational attempt frequencies among the different migration steps, shows that the migration of Sn is also controlled by the reduced untrapped vacancy concentration, and thus by the same factor of R as for the alloying elements (Mg, Si) in AA6061. Hence, the addition of ~ 100 at.ppm Sn only affects diffusional processes through the reduction of available vacancies in the matrix.

In summary, we have shown that a modification of excess vacancy motion by minute additions of Sn offers the long-sought solution to the negative effect of RT storage in Al-Mg-Si alloys, with great importance for the application of this group of lightweight alloys. The advantage in kinetics and/or achievable strength (indicated by arrows in Fig. 3) in the industrial production of Al-Mg-Si alloys will increase the freedom either to decrease the necessary heat treatment time by a factor of 6 or to increase the hardness by 10%. The methodology of buffering excess vacancies at low temperature such that they are available for diffusion on demand at a later time during processing at a higher temperature is in fact not limited to Sn additions to Al-Mg-Si alloys. The mechanism is expected to be possible using other solute elements as well, e.g., indium for Al-Mg-Si alloys, and in other metallic systems (e.g., Mg and Cu alloys) where key microstructural evolution processes are controlled by vacancy-mediated diffusion. Furthermore, the selection of suitable trace element additions can be guided by a combination of first-principles modeling and an understanding of achievable trace element solubility in the alloy, thereby providing new directions for advanced and accelerated development of new or improved metal alloys.

The authors thank the people at AMAG Rolling for the fruitful discussion and for providing the commercial alloy AA6061. We are also grateful to the Austrian Research

Promotion Agency (FFG) and AMAG Rolling for their financial support of this work. W. A. C. and M. F. F. acknowledge support from the US Army Research Office through the Grant No. W911NF-11-1-0353.

*stefan.pogatscher@mat.ethz.ch

- [1] C. Kammer, *Aluminium Handbook: Fundamentals and Materials* (Beuth, Berlin, 2011), Vol. 1.
- [2] I. Kovačs, E. Nagy, and J. Lendvai, *Acta Metall. Mater.* **20**, 975 (1972).
- [3] J. Banhart, C. S. T. Chang, Z. Q. Liang, N. Wanderka, M. D. H. Lay, and A. J. Hill, *Adv. Eng. Mater.* **12**, 559 (2010).
- [4] P. Brenner and H. Kostron, *Z. Metallkd.* **4**, 89 (1939).
- [5] A. Guinier, *Nature (London)* **142**, 569 (1938).
- [6] G. D. Preston, *Nature (London)* **142**, 570 (1938).
- [7] J. Banhart, M. D. H. Lay, C. S. T. Chang, and A. J. Hill, *Phys. Rev. B* **83**, 014101 (2011).
- [8] M. J. Starink, L. F. Cao, and P. A. Rometsch, *Acta Mater.* **60**, 4194 (2012).
- [9] S. Esmaeili, D. J. Lloyd, and W. J. Poole, *Acta Mater.* **51**, 3467 (2003).
- [10] C. D. Marioara, S. J. Andersen, J. E. Jansen, and H. W. Zandbergen, *Acta Mater.* **51**, 789 (2003).
- [11] M. Murayama and K. Hono, *Acta Mater.* **47**, 1537 (1999).
- [12] S. Pogatscher, H. Antrekowitsch, H. Leitner, T. Ebner, and P. J. Uggowitzer, *Acta Mater.* **59**, 3352 (2011).
- [13] H. W. Zandbergen, S. J. Andersen, and J. Jansen, *Science* **277**, 1221 (1997).
- [14] C. Wolverton, *Acta Mater.* **55**, 5867 (2007).
- [15] H. K. Hardy, *J. Inst. Met.* **78**, 169 (1950).
- [16] I. J. Polmear, *Mater. Sci. Forum* **13–14**, 195 (1987).
- [17] G. A. Edwards, K. Stiller, G. L. Dunlop, and M. J. Couper, *Acta Mater.* **46**, 3893 (1998).
- [18] See Supplemental Material at <http://link.aps.org/supplemental/10.1103/PhysRevLett.112.225701> for details on the solution treatment, reconstruction procedure of atom probe tomography data and the full thermodynamic model.
- [19] D. Blavette, A. Bostel, J. M. Sarrau, B. Deconihout, and A. Menand, *Nature (London)* **363**, 432 (1993).
- [20] T. F. Kelly, D. J. Larson, *Annu. Rev. Mater. Res.* **42**, 1 (2012).
- [21] M. K. Miller, A. Cerezo, M. G. Hetherington, and G. D. W. Smith, *Monographs on the Physics and Chemistry of Materials: Atom Probe Field Ion Microscopy* (Oxford University Press, Oxford, 1996).
- [22] G. Kresse and J. Furthmuller, *Phys. Rev. B* **54**, 11169 (1996).
- [23] H. J. Monkhorst and J. D. Pack, *Phys. Rev. B* **13**, 5188 (1976).
- [24] G. Mills, H. Jonsson, and G. K. Schenter, *Surf. Sci.* **324**, 305 (1995).
- [25] E. A. Marquis and J. M. Hyde, *Mater. Sci. Eng. R* **69**, 37 (2010).
- [26] T. Homma, M. P. Moody, D. W. Saxey, and S. P. Ringer, *Metall. Trans. A* **43**, 2192 (2012).
- [27] F. D. Fischer, J. Svoboda, F. Appel, and E. Kozeschnik, *Acta Mater.* **59**, 3463 (2011).
- [28] D. Simonovic and M. H. F. Sluiter, *Phys. Rev. B* **79**, 054304 (2009).
- [29] G. Fioeito, S. Ceresara, and T. Federighi, *Acta Metall. Mater.* **14**, 452 (1966).
- [30] M. Mantina, Y. Wang, L. Q. Chen, Z. K. Liu, and C. Wolverton, *Acta Mater.* **57**, 4102 (2009).